

https://doi.org/10.1070/QEL17662

Multicore optical fibre embedded Fabry–Perot sensing element of a bend sensor

O.N. Egorova, S.G. Zhuravlev, V.I. Pustovoy, S.L. Semjonov

Abstract. **We propose a new type of a sensing element of a sensor for measuring the bending direction and magnitude, based on fibre Fabry–Perot interferometers embedded in the cores of multicore optical fibre. The measured sensitivity to the bend radius is 81 pm/m^{-1}. It is found that this sensitivity can be increased by varying the diameters of the optical fibres forming the sensing element.**

Keywords: *Fabry–Perot interferometer, bend sensor, multicore optical fibre.*

Recently, directional bend sensors based on writing fibre Bragg gratings in the cores of multicore optical fibre have been actively developed [1–4]. These sensors can be used to monitor the state of objects, in robotics, and in aircraft construction [5]. Misalignment of some cores in multicore optical fibre results in strains, which, due to the bending of fibre, have different effect on fibre Bragg gratings written in different cores. This, in turn, leads to different shifts in the reflection spectra of the gratings, which makes it possible to determine the direction and radius of the fibre bend.

In some cases, Fabry–Perot interferometers formed directly in optical fibre cores can serve as an alternative to fibre Bragg gratings as sensor sensing elements [6–9]. To obtain such elements, a relatively simple technology can be employed [9], which does not require the use of such complex equipment and laser radiation sources that are necessary for the formation of fibre Bragg gratings. In addition, devices based on Fabry–Perot interferometers potentially have high temperature resistance [10], which is also of interest for their use at high temperatures, for example, for aircraft engines.

In this work, we describe for the first time a sensing element of a directional bend sensor fabricated on the basis of Fabry–Perot interferometers embedded in each of the cores of multicore optical fibre. To develop the sensor, we used a technology based on etching the fibre end-face and then splicing it in an electric discharge with the end-face of another fibre. The difference in mechanical strains in the cores during bending of multicore fibre causes a different change in the length of the Fabry–Perot interferometers in side cores, depending on the direction and radius of the fibre bend. The change in the reflection spectra of interferometers in different cores during the bending of multicore fibre makes it possible to determine the sensitivity to the bending radius.

Figure 1 shows a segment of a multicore fibre bent in the figure plane with a bending radius R. Each fibre core contains a Fabry–Perot interferometer; the initial length of each interferometer in an unbent fibre is L_0. Core C1 is located at the centre of the fibre cross section, with its axis coinciding with the fibre axis. The axes passing through the centres of two side cores C2 and C3 are located in the plane of Fig. 1. Since the axis of the central core coincides with the neutral line of the fibre that is not subjected to stretching or compression during bending, the length L_1 of interferometer FP1 in the central core does not change as a result of the fibre bend and correspond to its value L_0 in the unbent fibre. Core C2 is subjected to stretching when the fibre is bent, while core C3 is compressed. It follows from Fig. 1 that the interferometer elongation in side core C2 relative to the central core is

$$\Delta L = L_2 - L_1 = \frac{d}{R} L_0, \tag{1}$$

where d is the distance between the centres of the cores in the fibre cross section; and L_2 is the interferometer length in core C2.

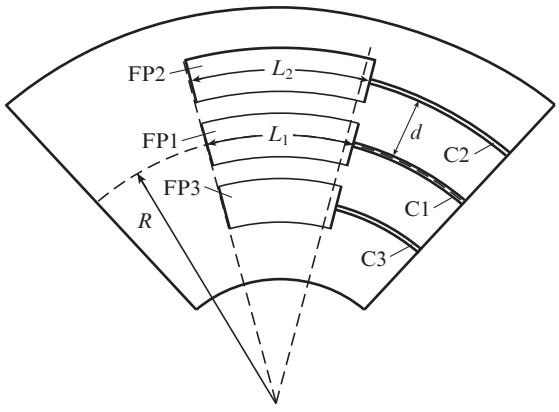

Figure 1. Multicore fibre with Fabry–Perot interferometers.

Since the reflection coefficient at the glass–gas interface is small (about 4%), the interferometers can be described using a two-beam model:

$$I = I_1 + I_2 + 2\sqrt{I_1 I_2}\cos\varphi,$$

O.N. Egorova, V.I. Pustovoy Prokhorov General Physics Institute of the Russian Academy of Sciences, ul. Vavilova 38, 119991 Moscow, Russia; e-mail: egorova@nsc.gpi.ru;
S.G. Zhuravlev, S.L. Semjonov Prokhorov General Physics Institute of the Russian Academy of Sciences, Dianov Fiber Optics Research Center, ul. Vavilova 38, 119333 Moscow, Russia

Received 26 October 2021
Kvantovaya Elektronika **51** (12) 1096–1100 (2021)
Translated by M.A. Monastyrskiy

where I_1 and I_2 are the intensities of waves reflected from two mirrors of the Fabry–Perot interferometer; $\varphi = 4\pi n L_{\text{int}}/\lambda$ is the phase difference of these waves; $n \approx 1$ is the refractive index of the gas medium inside the interferometer cavity; and L_{int} is the interferometer length. From the condition of the maximum $\varphi = 2\pi m$ in the reflection spectrum of the Fabry–Perot interferometer, where m is an integer, it follows that

$$\frac{\Delta L_{\text{int}}}{L_{\text{int}}} = \frac{\Delta\lambda}{\lambda}, \qquad (2)$$

where ΔL_{int} is an increase in the interferometer length, and $\Delta\lambda$ is a shift in the wavelength corresponding to one of the maxima in the reflection spectrum due to an increase in the interferometer length. From relations (1) and (2) we obtain $\Delta\lambda = (d/R)\lambda$.

Thus, the Fabry–Perot interferometer sensitivity to bending in side core C2 is $\Delta\lambda/(1/R) = d\lambda$. In core C3, which is subjected to compression due to bending, this value is also equal to $d\lambda$; in all other cores it takes intermediate values depending on the orientation angle of the fibre cross section relative to the bending direction. Consequently, the bending direction of fibre can be determined by the $\Delta\lambda$ value in different cores.

For the development of the sensor's sensing element, a seven-core fibre was selected, fabricated by a drilling method described, for example, in work [11]. A photograph of the end-face of a seven-core (A, B, C, D, E, F, G cores) fibre is shown in Fig. 2. Fibre cores have the same parameters and are arranged hexagonally. The distance between the centres of neighbouring cores is 40.5 μm, the core diameter is about 5.3 μm, and the difference between the refractive indices of the core and cladding is 0.015. The cutoff wavelength of the first higher mode of each of the cores lies in the range of 1.45–1.47 μm, the distribution diameter of the mode field of each of the cores at a wavelength of 1550 nm is 5.7 μm, and the diameter of the silica glass cladding is 125 μm.

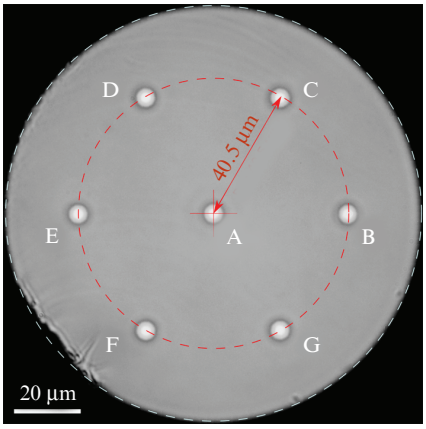

Figure 2. (Colour online) Photograph of a multicore fibre's end-face.

For the input/output of radiation from each core of a multicore optical fibre into/from single-core fibres, a small-size input/output device was manufactured [12, 11], allowing for sufficient mechanical robustness and low optical loss. This device provided a back reflection coefficient of less than −40 dB and optical insertion loss of less than 2 dB. The achieved values of optical loss and reflection coefficient were sufficient to conduct experiments on the development of a sensing element of the bend sensor.

Fibre embedded Fabry–Perot interferometers were fabricated using a method known for single-core fibres and described, for example, in work [9]. This method is based on the fact that the etching rate of doped silica glass exceeds the etching rate of undoped one. Therefore, when etching the fibre end-face, depressions are formed at the place where the cores of doped silica glass are located. During fusion splicing of the end-face of an etched multicore fibre with the end-face of an unetched fibre, depressions or voids on the end-face of the multicore fibre are converted into microcavities, which are Fabry Perot interferometers.

The external view of Fabry–Perot interferometers obtained in this way in a seven-core fibre is shown in Fig. 3. Figure 3a demonstrates Fabry–Perot interferometers formed by etching multicore fibre in hydrofluoric acid for 8 min. As a result of etching, the multicore fibre diameter decreased from 125 to 109 μm. A single-core fibre with an initial diameter of 125 μm was also etched to match the diameter of the multicore fibre. Figure 3b shows interferometers obtained by etching only multicore fibre for 5 min. It can be seen that the outer diameters of the optical fibres are different. The initial diameter of the multicore fibre was 125 μm; as a result of etching in hydrofluoric acid it decreased to 113 μm. The multi-core fibre was fusion spliced to single-core fibre with a diameter of 125 μm. A Fujikura FCM 80 S fusion splicer was used to form Fabry–Perot interferometers.

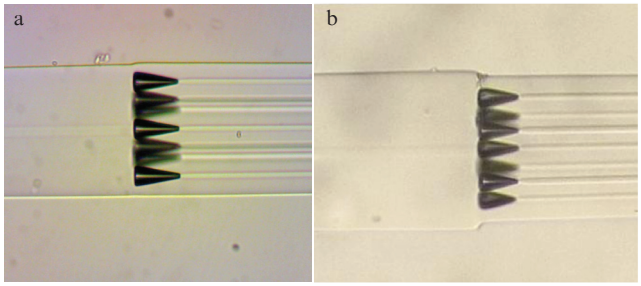

Figure 3. (Colour online) External view of Fabry–Perot interferometers in an element with (a) the same and (b) various fibre diameters.

The reflection spectrum of microcavities (Fabry–Perot interferometers) was studied in the scheme shown in Fig. 4. The radiation source was a Superlum SLD-76-MP semiconductor superluminescent diode (SLD) with a spectrum width of 50 nm (at a 3 dB level), centred in the vicinity of a wavelength of 1550 nm; the reflected signal was recorded using an ANDO AQ6317B optical spectrum analyser (OSA). The signal from the source was fed to the fibre-optic circulator input and alternately directed to each individual core of a multicore fibre (*2*) using the input/output device (*1*). Switching between the cores was performed using a fibre-optic connector (*6*).

To determine the sensitivity of the developed interferometers to the bending radius value, we measured the interferometer's reflection spectra in each core at various bending diameters of the fibre. To this end, a fibre segment with interferometers was placed on the cylindrical surface of a specially made support (*4*) in a groove. The groove depth was about 500 μm. To ensure a complete fit to the cylindrical surface, the fibre segments in the grooves were fixed with clips (*5*) in front

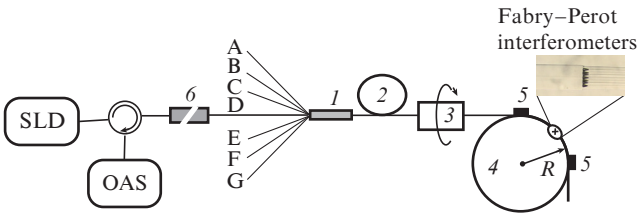

Figure 4. (Colour online) Schematic of the setup.

and behind the interferometers, as shown in Fig. 4. To change the cross-section orientation relative to the bending direction, the fibre was rotated using a rotary movable block (*3*). In this case, the fibre could rotate freely in the grooves. In each position of the movable block, the reflection spectra of the Fabry–Perot interferometers in each of the cores were recorded with a resolution of 0.5 nm.

In the measurements, the shift of one of the maxima of the reflection spectrum of each interferometer was determined at various fibre bending radii and various cross-section orientations relative to the bending direction. Figure 5a shows on a linear scale the reflection spectrum of an interferometer in one of the cores of the multicore fibre. When determining the reflection spectrum maximum, the superluminescent source spectrum was taken into account in accordance with the formula

$$I_i = I_i^{\mathrm{FP}} \frac{I_{\max}^{\mathrm{SLD}}}{I_i^{\mathrm{SLD}}},$$

where I_i is the intensity at the wavelength λ_i; I_i^{FP} is the intensity at the wavelength λ_i in the measured reflection spectrum of the interferometer; and $I_{\max}^{\mathrm{SLD}}$ and I_i^{SLD} are the maximum intensity and intensity at the wavelength λ_i in the superluminescent diode spectrum. The reflection spectrum of the interferometer is shown in Fig. 5b with allowance for the superluminescent source spectrum. The position of the spectrum maximum was determined using the centre of gravity (COG) algorithm [13, 14]: the wavelength λ_{m} corresponding to one of the reflection spectrum maxima was calculated by the formula

$$\lambda_{\mathrm{m}} = \sum_1^k I_i \lambda_i \Big/ \sum_1^k I_i,$$

where k is the number of points into which the spectrum interval is divided. The initial and final wavelengths λ_1 and λ_k correspond to an intensity close to the minimum (Fig. 5b).

First, the reflection spectra of interferometers were measured in an unbent fibre. The lengths L of the Fabry–Perot interferometers in various cores were determined by the difference in the wavelengths λ_1 and λ_2 of adjacent maxima in the obtained reflection spectra: $L = \lambda_1 \lambda_2/[2n(\lambda_1 - \lambda_2)]$, where $n \approx 1$. The interferometer lengths in various cores, calculated in accordance with the period of the reflected signal spectrum, ranged from 38 to 40.5 μm in an element with the same fibre diameters (Fig. 3a) and from 29 to 32.5 μm in an element with various fibre diameters (Fig. 3b).

Figure 6 shows the measured values of the wavelength shift of one of the maxima in the reflection spectra of each interferometer relative to the wavelength value in the unbent fibre for various bending directions. The angle between some initial and current orientation of the fibre cross section relative to the bending direction is plotted along the abscissa axis. Measurements were performed for an element with the same fibre diameters at bending radii of 20 and 6 cm. The position of the interferometer reflection spectrum maximum in the central core A does not change, while the positions of the reflection spectra maxima of the interferometers in the side cores B–G exhibit a sinusoidal dependence on the angle.

Figure 7a shows the dependence of the wavelength shift of one of the maxima in the reflection spectrum of interferometers in various cores on the fibre bending curvature $1/R$ at a fixed cross-section orientation angle relative to the bending direction for an element with the same fibre diameters. Measurements were performed for curvatures ranging from 0 to 20 m^{-1}. The largest shift in the reflection spectrum maximum is observed for the side cores E and B. The slope of the linear approximation of the dependence for core B is -82 pm/m^{-1} ($R^2 = 0.995$), while for core E it amounts to 81 pm/m^{-1} ($R^2 = 0.996$). Figure 7b shows similar dependences for an element with various fibre diameters. The largest wavelength shift in the reflection spectrum maximum is also observed for the side cores B and E. The linear approximation slope in the dependence for the core B is -97 pm/m^{-1} ($R^2 = 0.992$), while for the core E it is 100 pm/m^{-1} ($R^2 = 0.993$).

Thus, a decrease in the diameter of multicore fibre compared to single-core fibre leads to an increase in the sensitivity to the bending radius of the fibre. This can be explained as

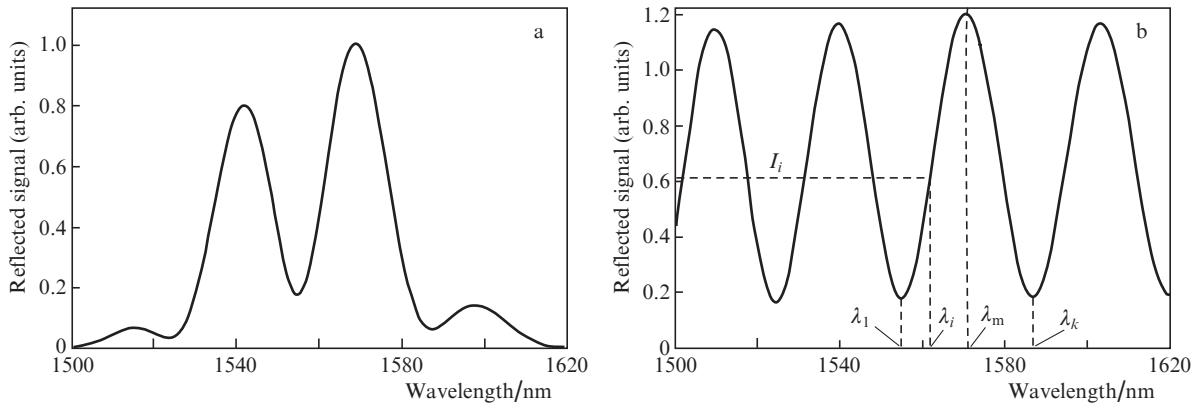

Figure 5. (a) Reflection spectrum of one of the Fabry–Perot interferometers and (b) reflection spectrum with allowance for the original spectrum of the SLD source.

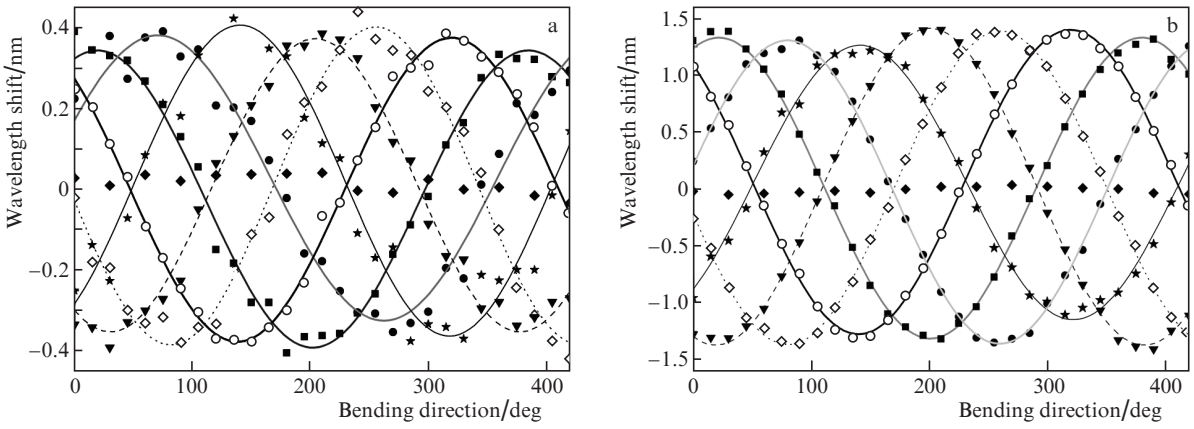

Figure 6. Wavelength shift in one of the maxima in the reflection spectra of each interferometer in an element with the same fibre diameters (Fig. 3a) relative to its value in the unbent optical fibre at bending radii of (a) 20 and (b) 6 cm for (♦) A, (■) B, (●) C, (★) D, (▼) E, (◇) F, and (○) G cores.

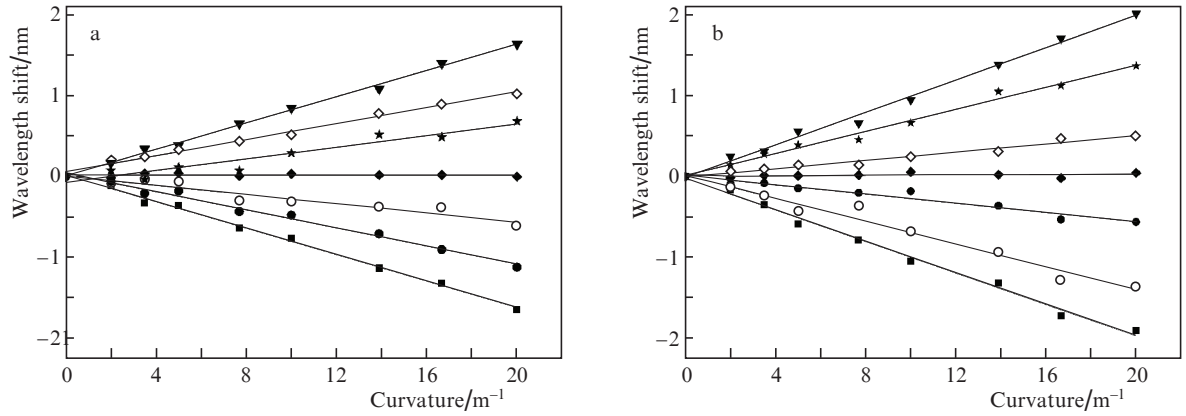

Figure 7. Wavelength shift in one of the maxima in the reflection spectrum of interferometers as a function of the bending curvature $1/R$ in the case of a fixed orientation angle of the fibre cross section relative to the bending direction at (a) the same (Fig. 3a) and (b) various (Fig. 3b) fibre diameters for (♦) A, (■) B, (●) C, (★) D, (▼) E, (◇) F, and (○) G cores.

follows. Let us draw two normal sections ab and a_1b_1 near the place where the fibre diameters change so that the cutout element has a small length (Fig. 8). The moment of elastic forces acting on one of the end-faces of the cutout element from the side of the fibre located to the left of the section ab must be balanced by the moment of elastic forces acting on the opposite end-face of the element from the side of the fibre located to the right of the section a_1b_1. The moment of elastic forces M can be calculated by the formula [15]

$$M = \frac{E}{R}\int_S \xi^2 \mathrm{d}S, \tag{3}$$

where E is Young's modulus; ξ is the coordinate of a point in the fibre cross section; and S is its cross-sectional area. The integral in (3) is determined by the shape and size of the fibre cross section (for a circular cross section it is equal to it $1/(4\pi r^4)$, where r is the fibre cross-section radius). Since the fibre radius in section ab (Fig. 8) is larger than the radius in section a_1b_1, to compensate for the moment of elastic forces, it is necessary that near the point of diameter change, fibre with a smaller diameter bends with a smaller bending radius R_1 than fibre with a larger diameter. In this case, the bending radius of a larger-diameter optical fibre near the splicing point of the fibres can increase compared to the radius R_0 of the cylindrical surface on which optical fibre is located. The described phenomenon leads to an increase in sensitivity due to the fact that the bending radius of smaller-diameter fibre in which the Fabry–Perot interferometers are located is less than the measured bending radius near the point of change in fibre diameters.

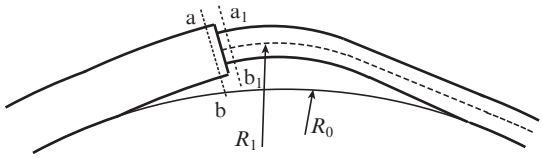

Figure 8. Bending of the splicing point of two optical fibres of various diameters.

The presence of Fabry–Perot interferometers also changes the cross-section shape of smaller-diameter fibre near the splicing point of the fibres. As a result, the integral in formula (3) decreases, which corresponds to a local increase in the bending radius of multicore fibre near the splicing point. This explains the difference between the measured sensitivity in the case of fibres of the same cross section from the calcu-

lated one, which at a distance of 40.5 μm between the centres of neighbouring cores is about 63 pm/m^{-1} at a wavelength of 1550 nm.

Since the reflection spectrum of the Fabry–Perot interferometer has rather wide maxima, the measurement error of the wavelength shift is greater than that in the case of fibre Bragg gratings, which leads to an unacceptably high measurement error for large bending radii. To improve the accuracy of measurements with a Fabry–Perot interferometer, it is necessary to use other signal processing algorithms based, for example, on the Fourier transform [16]. As shown in work [17], the minimum calculated error of measuring the interferometer length in this case can be 0.065 nm, while the experimentally obtained one is 0.18 nm. The bending radius corresponding to a change in the interferometer length by 0.18 nm is about 9 m at a distance of 40 μm between the centres of the cores and an interferometer length of 40 μm. To improve accuracy, the interferometer length and the distance between the cores can be increased: at a distance of 100 μm between the centres of the cores and an interferometer length of 100 μm, the bending radius corresponding to a 0.18 nm change in the interferometer baseline is approximately 55 m.

Limitations on the minimum allowable bending radius of the sensor may arise due to possible mechanical destruction of the fibre at the splicing point. During fusion splicing, certain rules must be observed, namely: removing the protective coating without damaging the fibre's glass surface (chemical dissolution of the polymer), fixing the fibre's end-faces in the fusion splicer in places with a protective coating, and avoiding mechanical contacts with the fibre section where the coating has been removed. In this case, the splicing joint strength lies in the range 2.1–2.8 GPa [18], which corresponds to the elongation of the fibre by 3%–4%. Such bending stretching in certain areas of the fibre surface may occur at the same ratio of the fibre radius to its bending radius. With a fibre diameter of 100 μm, the permissible radius of short-term (~1 s) bending of fibre at the splicing point is 1.25–1.7 mm. If a long bending is expected, it is desirable to reduce the permissible load by 3 times [19] and, accordingly, increase by 3 times the permissible minimum bending radius, i.e. up to 3.75– 5 mm. Even in this case, the limitations on splicing strength are not critical for most applications.

Thus, a sensing element of a directional sensor based on Fabry–Perot interferometers embedded in multicore optical fibre has been proposed and experimentally implemented. The difference in the change in the lengths of Fabry–Perot interferometers when fibre is bent, which occurs due to the difference in mechanical strains in the cores of multicore optical fibres, makes it possible to determine the direction and radius of bending. Fibre embedded interferometers have been developed by fusion splicing the end-face of multicore optical fibre pre-etched in hydrofluoric acid with the end-face of another fibre. In this case, cavities in the core region are formed due to the difference in the etching rates of the doped core glass and the undoped glass of the optical fibre cladding. The measured sensitivity of the sensor to the bending radius value was 81 pm/m^{-1}. We have also found that if the diameter of the optical fibre spliced to the multicore fibre exceeds the multicore fibre diameter, an increase in the sensitivity is observed as a result of a local increase in the bending radius of the multicore fibre near the splicing point.

Acknowledgements. This work was supported by the Center of Excellence "Center of Photonics" funded by the Ministry of Science and Higher Education of the Russian Federation under Contract 075-15-2020-912.

References

1. Gander M.J., MacPherson W.N., McBride R., Jones J.D.C., Zhang L., Bennion I., Blanchard P.M., Burnett J.G., Greenaway A.H. *Electron. Lett*., **36**, 120 (2000).
2. Bronnikov K., Wolf A., Yakushin S., Dostovalov A., Egorova O., Zhuravlev S., Semjonov S., Wabnitz S., Babin S. *Opt. Express*, **27**, 38421 (2019).
3. Butov O.V., Bazakutsa A.P., Chamorovskiy Yu.K., Fedorov A.N., Shevtsov I.A. *Sensors*, **19**, 4228 (2019).
4. Westbrook S., Kremp T., Feder K.S., Ko W., Monberg E.M., Wu H., Simoff D.A., Taunay T.F., Ortiz R.M. *J. Lightwave Technol*., **35**, 1248 (2017).
5. Amanzadeh M., Aminossadati S.M., Kizil M.S., Rakić A.D. *Measurement*, **128**, 119 (2018).
6. Cibula E., Donlagic D. *Opt. Express*, **15**, 8719 (2007).
7. Rao Y.J., Deng M., Duan D.W., Yang X.C., Zhu T., Cheng G.H. *Opt. Express*, **15**, 14123 (2007).
8. Villatoro J., Finazzi V., Coviello G., Pruneri V. *Opt. Lett*., **34**, 2441 (2009).
9. Machavaram V.R., Badcock R.A., Fernando G.F. *Sens. Actuators A*, **138**, 248 (2007).
10. https://technicasa.com/fabry-perot-sensors-filters/tfp10-micro-fabry-perot-strain-sensor-to-700c/.
11. Egorova O.N., Astapovich M.S., Belkin M.E., Semjonov S.L. *Quantum Electron*., **46**, 1134 (2016) [*Kvantovaya Elektron*., **46**, 1134 (2016)].
12. Li B., Feng Z., Tang M., Xu Z., Fu S., Wu Q., Deng L., Tong W., Liu S., Shum P.P. *Opt. Express*, **23**, 10997 (2015).
13. Villatoro J., Antonio-Lopez E., Schulzgen A., Amezcua-Correa R. *Opt. Lett*., **42**, 2022 (2017).
14. Ezbiri A., Kanellopoulos S.E., Handerek V.A. *Opt. Commun*., **150**, 43 (1998).
15. Sivukhin D.V. *Mekhanika: uchebnoe posobie dlya vuzov* (Mechanics: A Textbook for Universities) (Moscow: Nauka, 1989) p. 576.
16. Egorov S.A., Mamaev A.N., Likhachiev I.G. *Proc. SPIE*, **2594**, 193 (1995).
17. Miridonov S.V., Shlyagin M.G., Khomenko A.V., Spirin V.V. *Proc. SPIE*, **4777**, 136 (2002).
18. Krause J.T., Kurkjian C.R., Paek U.C. *Electron. Lett*., **17**, 232 (1981).
19. Bogatyrev V.A., Bubnov M.M., Dianov E.M., Rumyantsev S.D., Semjonov S.L. *Opt. Eng*., **30** (6), 690 (1991).